Synthesis and Characterization of Polyaniline/NiO Nanocomposite

B. H. Shambharkar, S. S. Umare

Department of Chemistry, Visvesvaraya National Institute of Technology, Nagpur 440 010, India

Received 9 June 2010; accepted 6 February 2011
DOI 10.1002/app.34286
Published online 10 June 2011 in Wiley Online Library (wileyonlinelibrary.com).

ABSTRACT: Spherical nickel oxide (NiO) nanoparticles were prepared by using nickel chloride as precursor in the ethylene glycol as solvent and urea as precipitant. The X-ray diffraction study showed that NiO has single-phase cubic structure with average crystallite size of 35 nm. The prepared NiO nanoparticles were incorporated into polyaniline (PANI) matrix during *in situ* chemical oxidative polymerization of aniline with different molar ratios of aniline: NiO (12 : 1, 6 : 1, and 3 : 1) at 5°C using $(NH_4)_2S_2O_8$ as oxidant in aqueous solution of sodium dodecylbenzene sulfonic acid, as surfactant and dopant under N_2 atmosphere. The synthesized composites have been characterized by means of X-ray diffraction (XRD), thermogravimetric analysis, Fourier transform infrared (FTIR), scanning electron microscopy, TEM, and vibrating sample magnetometer for its structural, thermal, morphological, and magnetic investigation. The XRD and FTIR studies show that the NiO particles are in the composite. The room temperature conductivities of the synthesized PANI, PANI/NiO (12 : 1), (6 : 1), and (3 : 1) composites were found to be 3.26×10^{-4}, 1.88×10^{-4}, 1.5×10^{-4}, and 4.61×10^{-4} S/cm, respectively. The coercivity (H_c) and remnant magnetization (M_r) of NiO, PANI/NiO NCs (12 : 1), (6 : 1), and (3 : 1) at 5 K was found to be 8.22×10^{-2}, 6.31×10^{-2}, 6.42×10^{-2}, 6.27×10^{-2} T, and 6.64×10^{-3}, 1.83×10^{-4}, 3.07×10^{-4}, and 3.98×10^{-4} emu/g, respectively. J Appl Polym Sci 122: 1905–1912, 2011

Key words: conducting polymers; nanoparticles; nanocomposites; magnetic properties

INTRODUCTION

Nanoparticles of transition metal oxides have been investigated by several workers in the last few years. The study of these nanoparticles has become of increasing interest due to the presence of unusual physical and chemical properties different from those observed in bulk materials. A reduction in particles size to nanometer scale results in various special properties such as the quantum size effects, the high surface area, and lower sintering temperature. Besides their structural aspects, magnetic properties of the oxide nanoparticles are of particular interest. Some reports[1] suggested that nickel oxide (NiO) nanoparticles exhibit weak ferromagnetism or superparamagnetism for the fine particles. Recently, Karthik et al.[2] have studied particle size effect on the magnetic properties of NiO nanoparticles of size range 16–25 nm. They observed that the particle size have strong influence on the magnetic properties of NiO nanoparticles. Smaller particles have large interface area between the ferromagnetic phase and antiferromagnetic matrix, and the structural disorder and exchange coupling increases with interface area. Bulk NiO has a cubic (NaCl-type) structure with a lattice parameter of 0.4177 nm and is classified as a Mott–Hubbard insulator with very low conductivity of the order of $10^{-11}\ \Omega^{-1}\ m^{-1}$ at room temperature.[3] However, the conductivity of NiO is drastically increased when prepared in the form of thin films or consolidated nanoparticles[4] (2.5–17 nm) due to the holes generated by Ni vacancies in the lattice. The electrical conduction is primarily ascribed to the hopping of holes associated with the Ni^{2+} vacancies.

NiO nanoparticles are *p*-type semiconducting[5] with band gap 3.51 eV. It is considered as promising electrode material for electrochemical capacitor[6] and gas sensor for NO_2, NH_3, and H_2.[7] NiO has received a considerable amount of attention for its catalytic properties such as decomposition of ammonium perchlorate,[8] hydrocracking reactions, reforming of hydrocarbons, and methane for production of syngas, the removal of tar followed by the adjustment of the gas composition in biomass pyrolysis/gasification, in cellulose pyrolysis, and so forth.[9] Several methods are reported for the preparation of NiO nanoparticles viz; biosurfactant-mediated microemulsion technique,[10] sol–gel method,[11] template-free synthesis.[12]

Polyaniline (PANI) is one of the most promising electrically conducting polymer of particular interest because of its various structures, special doping mechanism, environmental stability, high conductivity,[13–15]

Correspondence to: S. S. Umare (ssumare@chm.vnit.ac.in).

and its wide applications in microelectronic devices,[16] diodes,[17] light weight batteries,[18] super capacitors,[19] sensors,[20] corrosion inhibition,[21] and for electrorheological[22,23] and magnetorheological fluids.[24,25] Polymer nanocomposites (NCs) constitute a class of hybrid materials composed of a polymer matrix and an inorganic component, which has at least one dimension in the nanometer (<100 nm). The NCs exhibit combination of properties[26] like conductivity, electronic, electrochemical, catalytic, and optical properties. To obtain materials with synergetic advantage between PANI and inorganic nanoparticles, various composites of PANI with inorganic naonoparticles such as CeO_2,[27] TiO_2,[28,29] $BaTiO_3$,[30,31] MoO_3,[32] SnO_2,[33] Fe_3O_4,[34] Co_3O_4,[35] and NiO[36,37] are reported. Therefore, herein, an attempt has been made to generate novel NC intriguing electronic and magnetic properties by encapsulating the NiO particles with PANI matrix. These properties may arise due to physical as well as chemical interactions between the inorganic oxide surface and the organic material.[38]

In this communication, NiO nanoparticles were synthesized by the ethylene glycol (EG) route. EG works not only as solvent but also plays the role of a complexing and capping agent, which restrict the growth during the synthesis of nanoparticles. Second, it has high boiling point (197°C).[39,40] The synthesized NiO nanoparticles were incorporated in PANI matrix by *in situ* chemical oxidative polymerization of aniline in the presence of SDBS. SDBS helps in homogenous protonation of PANI and thereby improves its crystallinity, orientation, and electrical conductivity.[41] The structural, thermal, electrical, and magnetic properties of PANI/NiO NCs were compared to that of pristine PANI.

EXPERIMENTAL

Materials

Aniline (reagent grade, Merck) was distilled before use and stored at 10°C. Other reagents, dodecylbenzenesulphonic acid sodium salt (SDBS), ammonium persulphate, nickel chloride, urea, EG, and hydrochloric acid were of analytical grade and used as received. Double-distilled water was used for solution preparation.

Methods

Synthesis of NiO nanoparticles

NiO nanoparticles were prepared by EG route.[42,43] Fifty milliliters of nickel chloride (0.2*M*) solution were taken in three-necked RB flask fitted with air condenser. About 4.0 g urea and 150-mL EG was added. The reaction mixture was mixed properly and then refluxed at 160°C with continuous magnetic stirring for 6 h. The light green precipitate was obtained. The reaction mixture was kept for overnight. It was centrifuged, washed with methanol and acetone, and then dried at 100°C for 6 h in air oven. Finally, the product was calcined at 300°C for 3 h. Black/gray color powder was obtained.

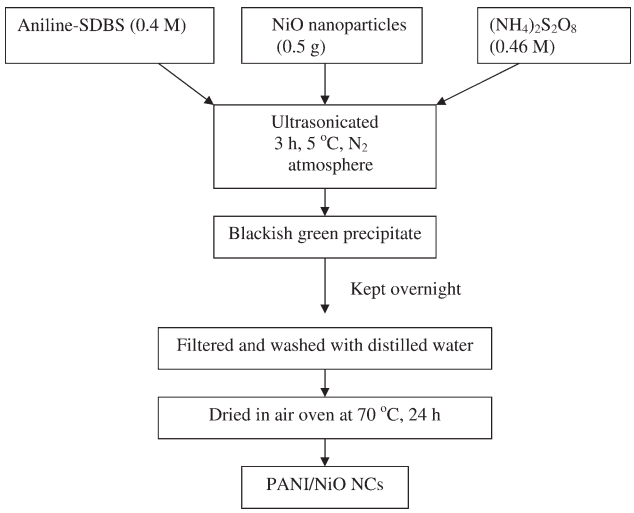

Scheme 1 Schematic representation of synthesis of PANI/NiO NCs.

Synthesis of PANI/NiO NCs

The PANI/NiO NCs (6 : 1) was prepared[34,35] by chemical-oxidative *in situ* polymerization of aniline. Precooled (~5°C) 100 mL solution containing 0.4*M* aniline and 0.08*M* SDBS was taken in four-necked flat-bottomed flask. Then 0.5 g as synthesized NiO nanoparticles was added to it. Precooled solution of ammonium persulphate (10.4972 g, 0.46*M*) was added slowly to the solution containing aniline, SDBS, and NiO nanoparticles. The polymerization was allowed to proceed in the presence of N_2 atmosphere at 5°C for 3 h with continuous sonication (Fs4, Frontline). The molar ratio of aniline: SDBS and aniline: APS was 5 : 1 and 1 : 1.15, respectively. The reaction mixture was equilibrated for overnight. The pH of aniline–SDBS solution was found to be nine before polymerization process. The blackish green precipitate of PANI/NiO composite was filtered and washed with distilled water till colorless filtrate was obtained and then it was dried at 70°C for 24 h. In the similar way, composites of different molar ratios (12 : 1, 3 : 1) of aniline to NiO have been prepared. Scheme 1 shows the schematic representation of synthesis of PANI/NiO composite.

Characterization

X-ray diffraction (XRD) analysis was conducted on X'Pert PRO, PANalytical X-ray diffractometer using

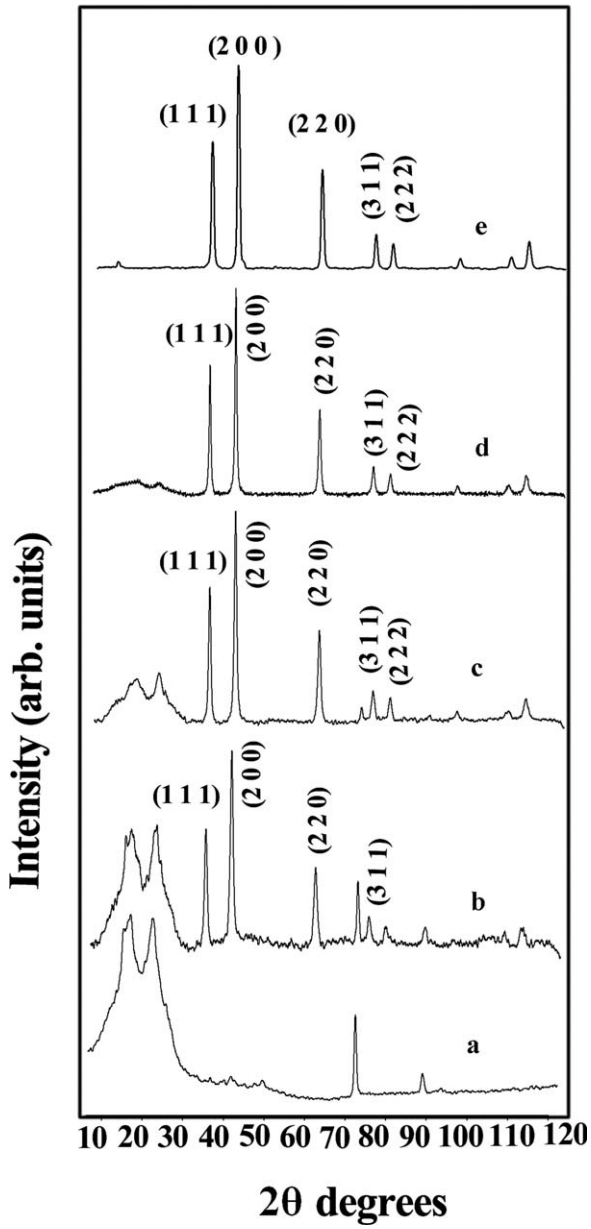

Figure 1 X-ray diffraction patterns of (a) PANI, (b) PANI/NiO (12 : 1), (c) PANI/NiO (6 : 1), (d) PANI/NiO (3 : 1), and (e) NiO.

Cu Kα radiation (λ = 1.5406 Å) at 45 kV and 40 mA. Measurements were performed in the 2θ range from 10° to 120°. Average crystallite size (t) of NiO particles was calculated from the line broadening using Scherrer's formula $t = 0.9\ \lambda/\beta\ \mathrm{Cos}\ \theta$, where β is the full width at half maximum of the strongest peak, λ is the X-ray wavelength (λ = 1.5406 Å), and θ is the angle of diffraction. Thermogravimetric analysis was performed on Pyris Diamond, Perkin–Elmer at the heating rate of 10°C/min in the temperature range from 30 to 1000°C under purging of argon atmosphere with flow rate 200 mL/min. Fourier transform infrared (FTIR) spectra were recorded on Perkin–Elmer FTIR spectrophotometer by using KBr pellet technique. FTIR measurements were taken from 4000 to 450 cm^{-1} with a 4.0 cm^{-1} resolution.

The surface morphology of the samples was examined from scanning electron microscopy (SEM) on JEOL JSA-840A equipped with an electron probe-microanalyzer system. Energy-dispersive X-ray (EDAX) measurement was also performed on the same equipment to determine chemical composition. Transmission electron microscopy images was obtained (TEM model CM 200 supertwin) at accelerating voltage of 200 kV and resolution of 0.2 nm. For TEM sample preparation, about 2 mg of powder sample was dispersed in 5 mL of methanol by sonication, and a drop of this solution was evaporated on a copper grid and then introduced into the sample chamber.

Electrical conductivity of compressed pellets of NCs was measured at frequency of 1 kHz at room temperature. The pellets were prepared with the help of hydraulic press (Kimaya Engineers, India) by

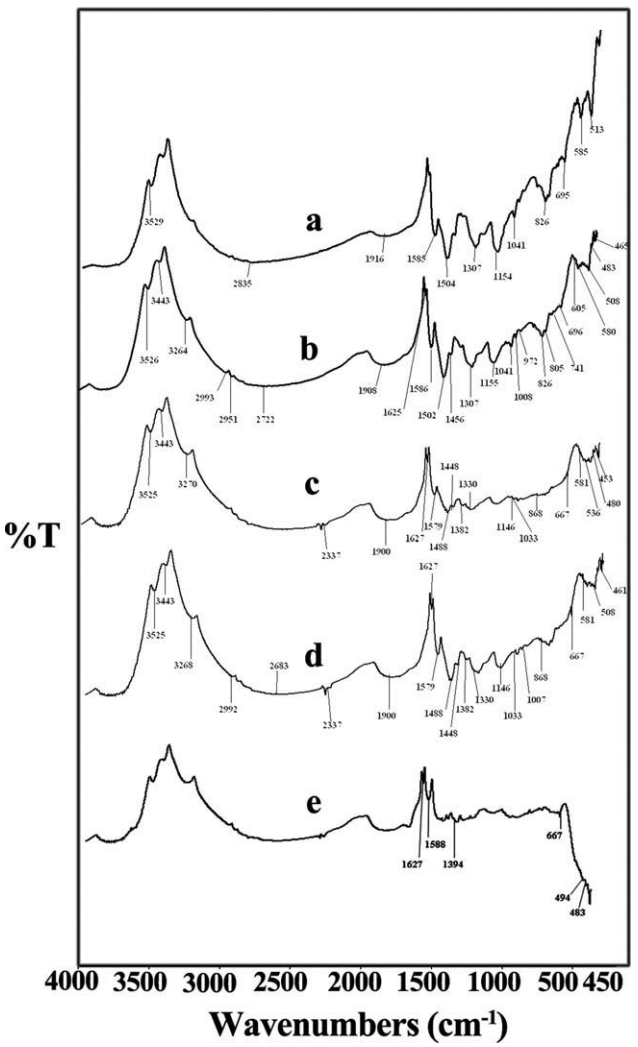

Figure 2 FTIR spectra of (a) PANI, (b) PANI/NiO (12 : 1), (c) PANI/NiO (6 : 1), (d) PANI/NiO (3 : 1), and (e) NiO.

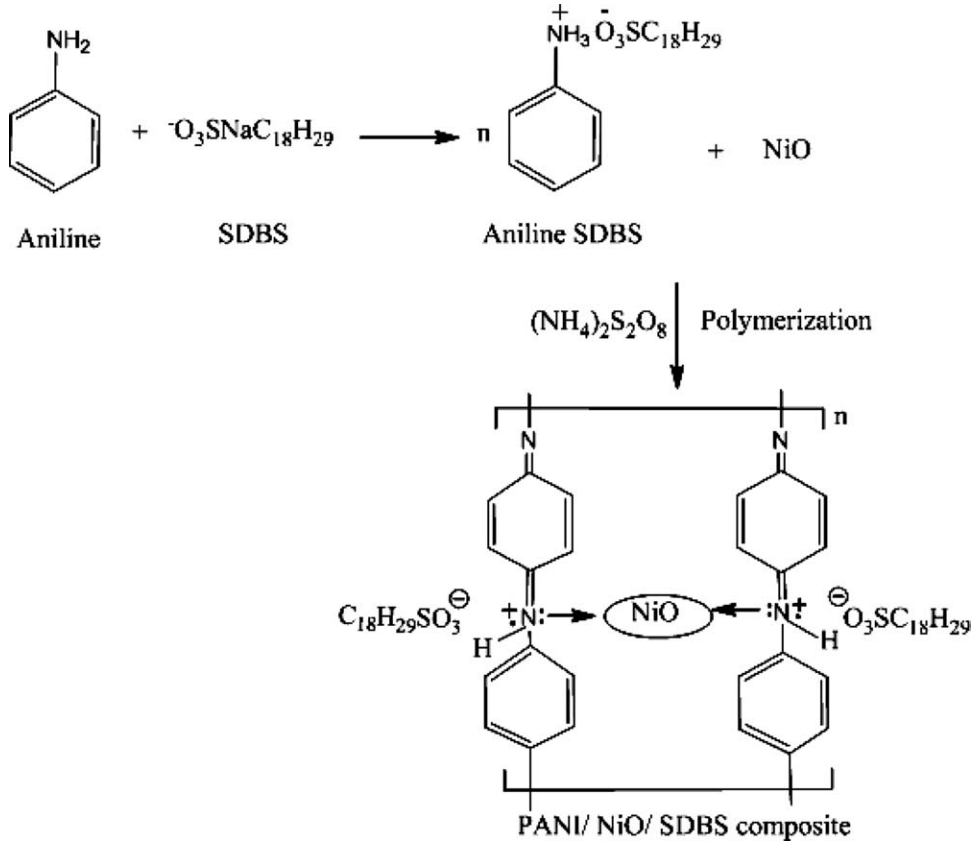

Scheme 2 Structure of PANI/NiO composite.

applying a pressure of 5000 kg/cm^2 for 30 s in steel die. These pellets were then subjected to D.C. resistivity measurements on 928 auto LCR Q tester (Systronics). The conductivity value was calculated from the measured resistance and sample dimensions. Magnetization measurements were performed on Vibrating Sample Magnetometer (VSM) Model oxford Maglab 14 T VSM.

RESULTS AND DISCUSSION

XRD study

X-ray diffraction (XRD) patterns of PANI, NiO, and PANI/NiO composites with different loadings of NiO are shown in Figure 1. The XRD pattern of the prepared NiO nanoparticles is in agreement with JCPDS file no. 73-1523, and the particles show cubic crystal system. The lattice constant of NiO from XRD data was found to be $a = 4.17$ Å, which is good agreement with JCPDS 04-0835 (4.1769 Å).[44] The average crystallite size of NiO particles was calculated by using Scherrer's relation was found to be 35 nm, which is consistent with the results of TEM. The XRD curve of PANI shows that PANI has partly crystalline structure, and the two broad peaks are observed at $2\theta = 20.41°$ and 25.61°. The XRD spectra of PANI/NiO NCs showed that the diffraction features appeared at about $2\theta = 37.20°$, 43.26°, 62.90°, 75.26°, and 79.25°, corresponding to the (1 1 1), (2 0 0), (2 2 0), (3 1 1), and (2 2 2) planes of the cubic phase of NiO, respectively. This indicates that the NiO particles are existing in the PANI/NiO NCs.

FTIR study

FTIR spectra of PANI, NiO, and PANI/NiO composites are shown in Figure 2(a–d). The FTIR spectrum of PANI [Fig. 2(a)] shows characteristic absorption bands[35,45,46] at 513, 826, 1041, 1154, 1307, 1504, and 1585 cm^{-1}. The bands at 1585 and 1504 cm^{-1} attributed to stretching vibrations of N=Q=N ring and N—B—N ring, respectively (where B refers to benzenic-type rings and Q refers to quinonic-type rings). The peak at 826 cm^{-1} is assigned to out-of-plane bending vibration of C—H on the 1,4-disubstituted aromatic rings. The peak at 1154 cm^{-1} assigned to C—N stretching of secondary aromatic amine. The peak at 1307 cm^{-1} may be due to the presence of the C—N$^{\bullet+}$ stretching vibration in protonic acid-doped PANI from SDBS–PANI, where SO_3 group of SDBS is bonded with N of PANI. The peak at 513 cm^{-1} is assigned to SO_3H of SDBS. Scheme 2 shows the structure of SDBS-doped PANI/NiO composites.

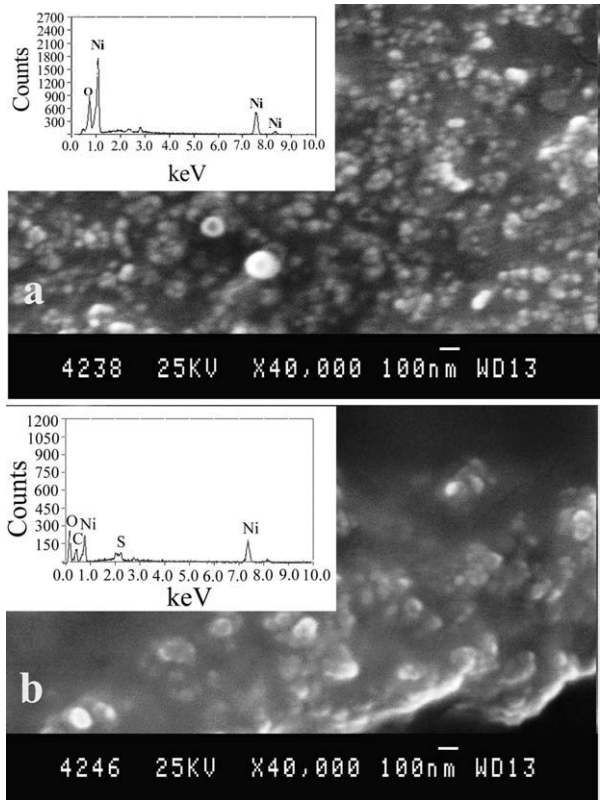

Figure 3 SEM images and EDAX pattern (inset) of (a) NiO and (b) PANI/NiO (3 : 1).

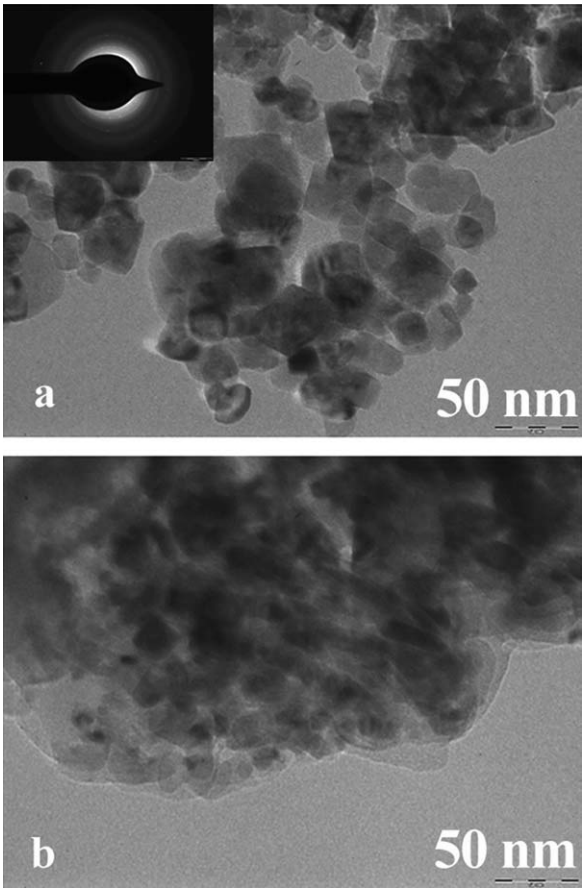

Figure 4 TEM images of (a) NiO and electron diffraction pattern (inset) and (b) PANI/NiO (6 : 1).

The similar absorption bands (PANI) are observed in PANI/NiO with a slight shift. The absorption bands due to stretching vibrations of N=Q=N (1579 cm^{-1}) and N—B—N rings (1488 cm^{-1}) are shifted to lower wavelengths in composites. It is likely that there is a weak intercalation between PANI and surface of NiO nanoparticles. The spectrum [Fig. 2(e)] shows the characteristic absorption bands of Ni—O vibrations[47] at 667 cm^{-1}. This absorption band is also seen in the composites.

Morphological studies

Figure 3(a,b) shows SEM images of the NiO and PANI/NiONCs. SEM images indicated that the prepared NiO nanoparticles have spherical morphology. Transmission electron microscopy of PANI/NiO NCs [Fig. 4(a,b)] elucidated further that NiO nanoparticles (35 nm) exist spherically in the PANI matrix. EDAX spectra of NiO and PANI/NiO (3 : 1) are shown in the inset of Figure 3. Elemental data are presented in Table I.

Thermal studies

The TG thermograms of NiO, PANI, and PANI/NiO are shown in Figure 5(a–e). NiO undergoes two-step degradation. PANI shows three-step weight loss.[34,48] The initial weight loss up to ~105°C is due to residual water, loss above 200°C may be due to loss of SDBS, and thermal degradation of PANI started after 300°C. PANI/NiO NCs shows similar decomposition steps of PANI but it has high stability. To compare the relative thermal stability of NiO, PANI, and PANI/NiO, % weight loss at different temperatures are reported in Table II. From Table II, it is observed that PANI/NiO (3 : 1) is more thermally stable compared to PANI, and, on increasing the percentage of NiO in composite, the thermal stability of composite is increasing due to more incorporation of inorganic component. The similar results were reported by Qi et al.[37] DTA curve of NiO, PANI, and PANI/NiO composites is shown in Figure 6(a–

TABLE I
Elemental Analysis Data of PANI, NiO, and PANI/NiO NCs

Samples	C %	N %	S %	O %	Ni %
NiO	–	–	–	9.53	90.47
PANI	36.15	43.49	8.92	11.44	–
PANI/NiO (12 : 1)	39.96	40.84	8.60	6.3	4.30
PANI/NiO (6 : 1)	37.13	35.91	5.00	9.32	12.00
PANI/NiO (3 : 1)	34.02	22.43	3.36	9.17	31.02

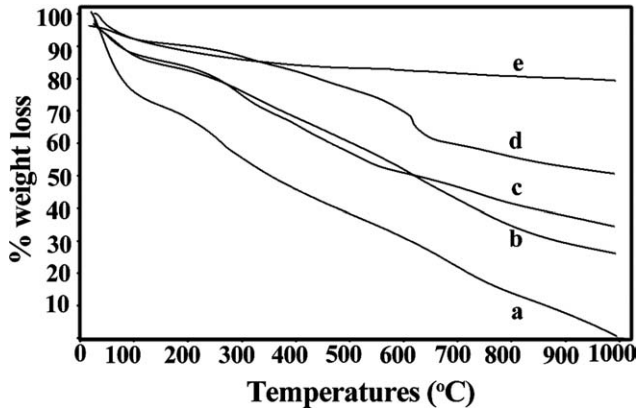

Figure 5 TG thermogram of (a) PANI, (b) PANI/NiO (12 : 1), (c) PANI/NiO (6 : 1), (d) PANI/NiO (3 : 1), and (e) NiO.

e). NiO has endothermic peak at 500°C, which may be due to partial reduction of NiO to Ni metal. The similar endothermic peak is found in PANI/NiO (3 : 1) at 580°C.

Electrical and magnetic properties

The NiO content affects significantly on both conductivity and magnetization of the resulting PANI composites. PANI shows the room temperature conductivity 3.26×10^{-4} S/cm and those for PANI/NiO (12 : 1), (6 : 1), and (3 : 1) composites are 1.88×10^{-4}, 1.5×10^{-4}, and 4.61×10^{-4} S/cm, respectively. The reported value of electrical conductivity of pure PANI (acid free) and SDBS-doped PANI is 1.8×10^{-10} and 1.2×10^{-2} S/cm, respectively.[49] Conductivity varies with degree of protonation and kind of acid dopant. Song et al.[36] have synthesized PANI/NiO in SDBS micelles with nanorods of lengths about 200–500 μm, width about 3–5 μm, and thickness about 40–96 nm. The conductivity for usual PANI and that for composite material PANI/NiO/SDBS was found to be 1.05×10^{-4} S/cm and 2.2×10^{-3} S/cm, respectively. Rectangular tubes[50] of PANI/NiO composites of various sizes from a nanometer to a micrometer were synthesized by changing the molar ratio of aniline/NiO 1 : 64, 1 : 48, and 1 : 32. The conductivity of PANI nanorods was 1.0×10^{-3} S/cm and that of PANI/NiO rectangular microtubes was 2.3×10^{-2}, 6.8×10^{-2}, and 0.11 S/cm, respectively. In our study at a low-NiO concentration, the conductivity of PANI/NiO (12 : 1) and (6 : 1) composites is lower than PANI (Table III). This decreased in conductivity may be due to partial blockage of conductive paths by the NiO nanoparticles embedded in the PANI/NiO matrix. At a high dosing of NiO, the electrical conductivity of PANI–NiO (3 : 1) is more compared to pure PANI which

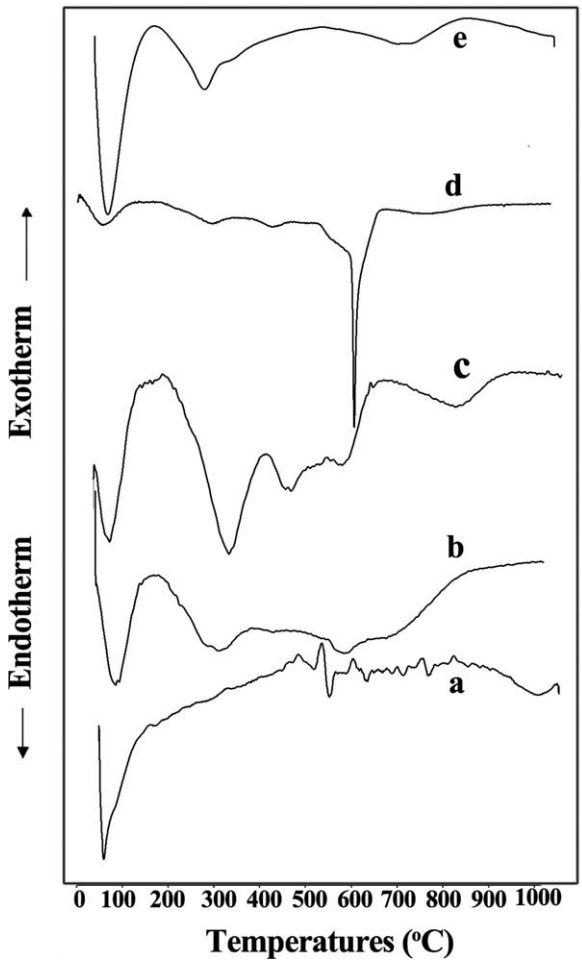

Figure 6 DTA curves of (a) NiO, (b) PANI/NiO (12 : 1), (c) PANI/NiO (6 : 1), (d) PANI/NiO (3 : 1), and (e) PANI.

TABLE II
% Weight Loss Data for PANI, NiO, and PANI/NiO Composites at Different Temperatures

Samples	% Weight loss (°C)			
	110	300	500	700
PANI	25.37	44.66	71.42	77.55
NiO	8.58	14.60	17.88	18.94
PANI/NiO (12 : 1)	10.56	22.29	39.29	58.54
PANI/NiO (6 : 1)	10.85	22.47	40.20	50.82
PANI/NiO (3 : 1)	3.97	14.75	20.66	38.81

TABLE III
Room Temperature Conductivity and Magnetic Parameters of PANI, NiO, and PANI/NiO NCs Measured at 5 K

Samples	Conductivity (S/cm)	M_r (emu/g)	H_c (T)
NiO	–	6.64×10^{-3}	8.22×10^{-2}
PANI	3.26×10^{-4}	6.02×10^{-5}	6.51×10^{-2}
PANI/NiO (12 : 1)	1.88×10^{-4}	1.83×10^{-4}	6.31×10^{-2}
PANI/NiO (6 : 1)	1.5×10^{-4}	3.07×10^{-4}	6.42×10^{-2}
PANI/NiO (3 : 1)	4.61×10^{-4}	3.98×10^{-4}	6.27×10^{-2}

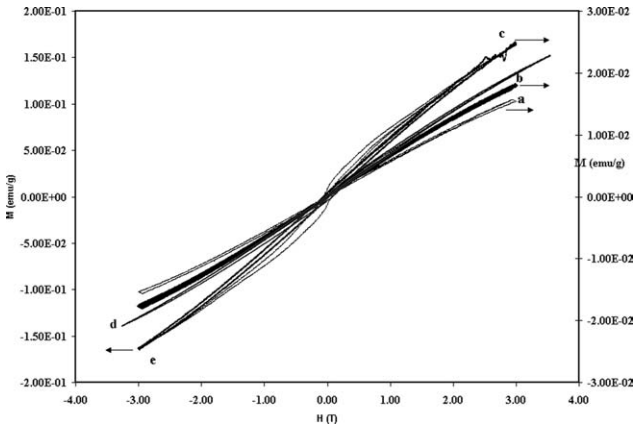

Figure 7 Magnetization versus applied field at 5 K for (a) PANI, (b) PANI/NiO (12 : 1), (c) PANI/NiO (6 : 1), (d) PANI/NiO (3 : 1), and (e) NiO.

may result from the increasing doping level of PANI with NiO, and the similar type of result was reported by Han et al.[50] and Song et al.[51] in their study.

The magnetization results are shown in Figure 7. Maximum applied field was up to 3 T. Under applied magnetic field PANI and NiO, PANI/NiO composite shows the positive magnetizations. The magnetization shows no sign of saturation even at the applied field of 3T. NiO nanoparticles exhibit ferromagnetic like behavior with hysteresis loop at 5K and has coercivity (H_c) = 8.22 × 10^{-2} T and remnant magnetization (M_r) = 6.64 × 10^{-3} emu/g, whereas PANI is paramagnetic. At lower temperatures, the spins are freezing, the system suffers from the Peierls instability, and thus the electrons are localized giving rise to a metal–semiconducting transition and an associated paramagnetism.[52] The M_r of PANI/NiO composites is found to be increased with increasing the concentration of NiO, and H_c values are decreased in the composites compared to PANI (Table III). At a low-NiO concentration, PANI/NiO (12 : 1) and (6 : 1) composites exhibit paramagnetic character that arises from the metal oxide–organic matrix, and at high dosing of NiO in the composite PANI–NiO (3 : 1), a small hysteresis loop was appeared that leads to ferromagnetism.

CONCLUSIONS

PANI/NiONCs have been successfully prepared by incorporating NiO nanoparticles into the PANI matrix. The incorporation of NiO into PANI matrix affects the conductivity, magnetic properties, and thermal stability of NCs. It is seen that the electrical and magnetic properties of the composite depend on the size and concentration of NiO in the composite. Thermogravimetric results reveal that NiO nanoparticles could improve the composite thermal stability possibly due to the molecular level interaction of NiO nanoparticles and PANI backbone. SEM and TEM images display that NiO nanoparticles exist spherically in the PANI matrix.

The authors acknowledge Department of Condensed Matter Physics and Material Science, TIFR Mumbai for VSM measurements. One of the authors B. H. Shambharkar is thankful to Director, Visvesvaraya National Institute of Technology Nagpur for awarding research fellowship.

References

1. Ichiyanagi, Y.; Wakabayashi, N.; Yamazaki, J.; Yamada, S.; Kimishima, Y.; Komatsu, E.; Tajima, H. Phys B 2003, 329–333, 862.
2. Karthik, K.; Selvan, G. K.; Kanagaraj, M.; Arumugam, S.; Jaya, N. V. J Alloy Comp 2011, 509, 181.
3. Makhlouf, S. A.; Kassem, M. A.; Abdel-Rahim, M. A. J Mater Sci 2009, 44, 3438.
4. Biju, V.; Khadar, M. A. Mater Res Bull 2001, 36, 21.
5. Li, X.; Zhang, X.; Li, Z.; Qian, Y. Solid State Commun 2006, 137, 581.
6. Liu, X.-M.; Zhang, X.-G.; Fu, S.-Y. Mater Res Bull 2006, 41, 620.
7. Wu, L.; Wu, Y.; Wei, H.; Shi, Y.; Hu, C. Mater Lett 2004, 58, 2700.
8. Wang, Y.; Zhu, J.; Yang, X.; Lu, L.; Wang, X. Thermochim Acta 2005, 437, 106.
9. Fen, L. J.; Bo, X.; Juan, D. L.; Rong, Y.; David, L. T. J Fuel Chem Technol 2008, 36, 42.
10. Palanisamy, P.; Raichur, A. M. Mater Sci Eng C 2009, 29, 199.
11. Thota, S.; Kumar, J. J Phys Chem Solids 2007, 68, 1951.
12. Liu, J.; Du, S.; Wei, L.; Liu, H.; Tian, Y.; Chen, Y. Mater Lett 2006, 60, 3601.
13. Jia, Q.; Shan, S.; Jiang, L.; Wang, Y. J Appl Polym Sci 2010, 26, 115.
14. Majid, K.; Awasthi S.; Singla, M. L. Sensor Actuators A 2007, 135, 113.
15. Li, W.; Wan, M. Synth Met 1998, 92, 121.
16. Nandi, M.; Gangopadhaya, R.; Bhaumik, A. Micropor Mesopor Mater 2008, 109, 239.
17. Zhao, C.; Xing, S.; Yu, Y.; Zhang, W.; Wang, C. Microelectron J 2007, 38, 316.
18. Dalas, E.; Vitoratos, E.; Sakkopoulos, S.; Malkaj, P. J Power Sources 2004, 128, 319.
19. Ryu, K. S.; Lee, Y.; Han, K.-S.; Park, Y. J.; Kang, M. G.; Park, N.-G.; Chang, S. H. Solid State Ionics 2004, 175, 765.
20. Manigandan, S.; Jain, A.; Majumder, S.; Ganguly, S.; Kargupta, K. Sensor Actuators B 2008, 133, 187.
21. Armelin, E.; Pla, R.; Liesa, F.; Ramis, X.; Irbarren, J.; Alemán, I. C. Corros Sci 2008, 50, 721.
22. Kim, S. G.; Lim, J. U.; Sung, J. H.; Choi, H. J.; Seo, Y. Polymer 2007, 48, 6622.
23. Fang, F. F.; Lee, B. M.; Choi, H. J Macromol Res 2010, 18, 99.
24. Kim, J. H.; Fang, F. F.; Choi, H. J.; Seo, Y. Mater Lett 2008, 62, 2897.
25. Fang, F. F.; Kim, J. H.; Choi, H. J. Polymer 2009, 50, 2290.
26. Reddy, K. R.; Lee, K. P.; Gopalan, A. I. Colloid Surf A 2008, 320, 49.
27. He, Y. Mater Chem Phys 2005, 92, 134.
28. Radhakrishnan, S.; Siju, C. R.; Mahanta, D.; Patil, S.; Madras, G. Electrochim Acta 2009, 54, 1249.
29. Fang, F. F.; Sung, J. H.; Choi, H. J. J Macromol Sci Phys 2006, 45, 923.
30. Fang, F. F.; Kim, J. H.; Choi, H. J.; Seo, Y. J Appl Polym Sci 2007, 105, 1853.
31. Fang, F. F.; Choi, H. J. J Mater Sci 2006, 41, 5782.

32. Wei, X.; Jiao, L.; Sun, J.; Liu, S.; Yuan, H. J Solid State Electrochem 2010, 14, 197.
33. Ze-qiang, H.; Li-zhi, X.; Wen-ping, L.; Xian-ming, W.; Shang, C.; Ke-long, H. J Cent South Univ Technol 2008, 15, 214.
34. Umare, S. S.; Shambharkar, B. H.; Ninghthoujam, R. S. Synth Met 2010, 160, 1815.
35. Shambharkar, B. H.; Umare, S. S. Mater Sci Eng B 2010, 175, 120.
36. Song, G.; Bo, J.; Guo, R. Colloid Polym Sci 2005, 283, 677.
37. Qi, Y.; Zhang, J.; Qiu, S; Sun, L; Xu, F.; Zhu, M.; Ouyang, L.; Sun, D. J Therm Anal Calorim 2009, 98, 533.
38. Reddy, K. R.; Lee, K. P.; Iyengar, A. G. J Appl Polym Sci 2007, 104, 4127.
39. Palchik, O.; Zhua, J.; Gedanken, A. J Mater Chem 2000, 10, 1251.
40. Jiang, X.; Wang, Y.; Herricks, T.; Xia, Y. J Mater Chem 2004, 14, 695.
41. Palaniappan, S.; John, A. Prog Polym Sci 2008, 33, 732.
42. Umare, S. S.; Ningthoujam, R. S.; Sharma, S. J.; Shrivastava, S.; Kurian, S.; Gajbhiye, N. S. Hyperfine Interact 2008, 184, 235.
43. Ningthoujam, R. S.; Gajbhiye, N. S.; Ahmad, A.; Umare, S. S.; Sharma, S. J. J Nanosci Nanotech 2008, 8, 3059.
44. Xu, C.; Hong, K.; Liu, S.; Wang, G.; Zhao, X. J Cryst Growth 2003, 255, 308.
45. Ghabari, K. H.; Mousavi, M. F.; Shamsipur, M.; Rahmanifar, M. S.; Heli, H. Synth Met 2006, 156, 911.
46. Aphesteguy, J. C.; Jacobo, S. E. Phys B 2004, 354, 224.
47. Qiao, H.; Wei, Z.; Yang, H.; Zhu, L.; Yan, X. J Nanomater 2009, 795928, 1.
48. Shi, Q.; Zhang, Y.; Jing, G.; Kan, J. Iran Polym J 2007, 16, 337.
49. Stejskal, J.; Prokeš, J.; Trchová, M. React Funct Polym 2008, 68, 1355.
50. Han, J.; Song, G.; Guo, R. J Polym Sci 2005, 44, 4229.
51. Song, G.; Han, J.; Guo, R. Synth Met 2007, 157, 170.
52. Dallas, P.; Stamopoulos, D.; Boukos, N.; Tzitzios, V.; Niarchos, D.; Petridis, D. Polymer 2007, 48, 3162.